ARCHIVES OF ELECTRICAL ENGINEERING VOL. 71(2), pp. 325–342 (2022)

DOI 10.24425/aee.2022.140714

Distributed collaborative optimization DC voltage control strategy for VSC–MTDC system with renewable energy integration

JINGYE LI[1] ✉, HAIYING DONG[1,2]

[1] *School of Automation and Electrical Engineering, Lanzhou Jiaotong University China*

[2] *School of New Energy and Power Engineering, Lanzhou Jiaotong University China*

e-mail: ✉*2516479670@qq.com, hydong@mail.lzjtu.cn*

(Received: 15.07.2021, revised: 08.11.2021)

Abstract: Aiming at the problem of DC voltage control deviation and instability caused by a large-scale renewable energy access VSC–MTDC system, this paper combines voltage margin control and droop control. A strategy for controlling collaborative optimization in a sparsely distributed communication network has been proposed. Firstly, the distributed modeling of the system is carried out by combining MAS technology with small signal modeling. Then, a distributed model predictive controller is designed for a single droop control converter station. On this basis, a distributed cooperative optimization control strategy is proposed. According to the DC voltage deviation, the system adopts different control methods to control the receiving converter station. Finally, based on PSCAD/EMTDC and MATLAB co-simulation platforms, a six-terminal flexible HVDC system is built to verify the effectiveness of the control strategy under different conditions such as input power fluctuation, any converter station out of operation and system communication failure.

Key words: DC voltage control, distributed model prediction, droop control, VSC–MTDC, PSCAD/EMTDC

1. Introduction

Recently, with the traditional energy crisis, the large-scale development and utilization of renewable energy such as wind energy and solar energy has become a research hotspot. However, the wind farms and photovoltaic power stations are geographically dispersed and far away from the load center, which grid and consumption become the bottleneck problem [1]. The Voltage Source

Converter Multi-Terminal Direct Current (VSC–MTDC) system connects multiple wind farms, photovoltaic power stations, DC power grids and AC systems through multiple VSC converter station ports. With the advantages of the conventional HVDC system one can achieve multiple power supply and power receiving multiple links, and there is no single point of failure [2–4]. However, in the MTDC system of renewable energy access, the randomness and volatility of renewable energy such as wind energy, solar energy have caused dynamic DC voltage stability problems, which in turn affect the stable operation of DC grids [5].

At present, the common coordinated control strategies of the MTDC system include master-slave control strategy [6], voltage margin control strategy [7] and droop control strategy [8]. The master-slave control strategy can achieve better DC voltage control, but it depends on the communication system. The voltage margin control strategy acts as an improved master-slave control policy, which does not rely on the high-speed communication system, however, the voltage margin setting process is complex, and the margin selection is not properly affected, as well as the DC voltage stability has a great influence. The droop control strategy allows multiple converter stations to participate in the coordinated control of the system at the same time, which can realize the rapid distribution of unbalanced power and stabilize the DC grid voltage, but it is worse control.

DC voltage is an important indicator to measure the stable operation of the MTDC system, and its control performance directly affects the stability of the system. Therefore, the optimal control of DC voltage in the MTDC system is the focus of current research [9,10]. Considering that the droop coefficient of traditional DC voltage control is fixed and cannot adapt to the scenario of frequent fluctuation of input power of the DC grid, references [11,12] proposed an adaptive droop control (ADC) strategy, but the droop coefficient calculation is complex, and frequent adjustment of the droop coefficient will cause the stability of DC voltage. Reference [13] proposed a flexible droop control strategy, which avoided system control problems caused by improper droop coefficient setting. In addition, references [14, 15] combined different cooperative control strategies and proposed a hybrid coordinated control strategy. In reference to the defects of the master-slave control strategy and the voltage droop control strategy with dead zones, reference [16] proposed a distributed DC voltage control strategy, and its dynamic response characteristics are good. The above control strategy does not need communication, which can reduce the system dependence on communication. However, the droop control converter station realizes the system control by local DC voltage measurement, the DC voltage control accuracy is not high, and the global control effect is not good.

Model predictive control (MPC) can effectively overcome the uncertainty and nonlinearity in the system. Recently, it has been widely used in the field of MTDC system optimization control. Reference [17] proposes an MMC control scheme based on MPC, which improves the system response speed and reduces the fluctuation of DC voltage, but the DC voltage still has a large deviation. Reference [18] proposed an MPC-based MTDC power grid controller, but the controller needs the information of each converter station to work and has a strong dependence on communication. The VSC–MTDC system with renewable energy access is a typical high-order multi-input and multi-out distributed system, and its internal control loops have complex coupling relationships [19], which leads to the poor dynamic control effect of centralized model predictive control on DC voltage of the system. Distributed model predictive control (Di-MPC) has the advantages of high reliability, flexibility and fast computation speed, which is especially suitable for the coordinated control of the VSC–MTDC system with renewable energy access.

2. Distributed model of VSC–MTDC system

Aiming at the distributed modeling of the VSC–MTDC system, first of all, this paper divides the VSC–MTDC system into several subsystem areas. Then, the distributed modeling method combining multi-agent technology and small signal modeling is adopted to carry out the distributed modeling of the system from the cyber layer and the physical layer. The structure diagram of the distributed modeling of the VSC–MTDC system is shown in Fig. 1.

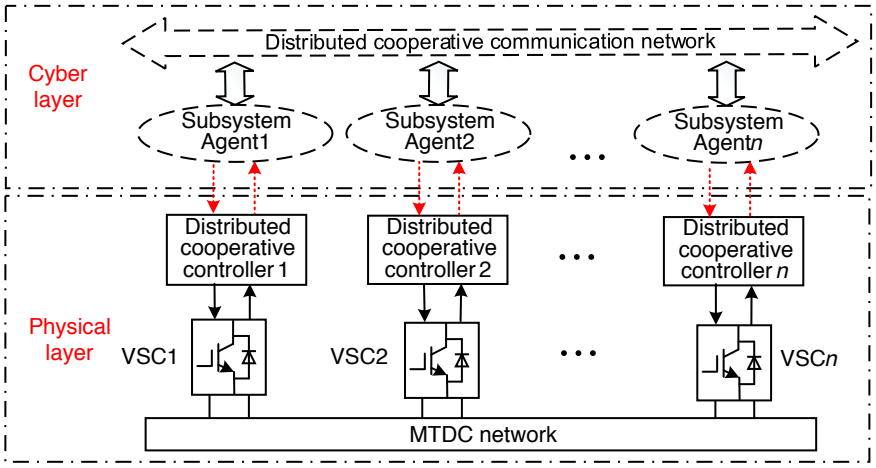

Fig. 1. Distributed modeling structure diagram of VSC–MTDC system

In the process of distributed modeling, the cyber layer applies MAS technology for modeling, which uses a single agent to simulate each subsystem area of the VSC–MTDC system, and realizes the information interaction between the agents through the sparsely distributed collaborative communication network. In the physical layer modeling, the small signal modeling method is used for each subsystem area of the VSC–MTDC system, which is mainly from three parts of the AC measurement model, DC network model and controller model of the receiving converter station, and finally establishes a regional model of the substation of a general receiving converter station.

2.1. Modeling based on multi-agent technology

In order to study the distributed model predictive voltage control of the VSC–MTDC system, this paper focuses on the distributed modeling of the receiving converter station. In the cyber layer, multi-agent technology is used to set the agent model, in which AgentH represents the main converter station subsystem, Agent1 represents the GSVSC1 droop control converter station, Agent2 represents the GSVSC2 droop control converter station, Agent*n* represents the GSVSC*n* droop control converter station. The distributed cooperative communication network topology of the multi-agent system is shown in Fig. 2. The red dotted connection between the two nodes indicates that there is information transfer between the two converter stations, and the arrow indicates the direction of the information transfer.

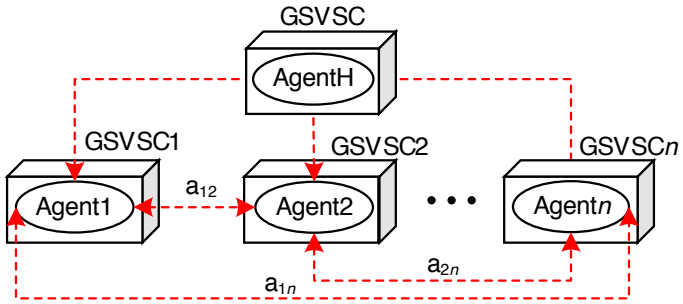

Fig. 2. Topology of distributed cooperative communication network

In the cyber layer modeling, the undirected graph $\boldsymbol{G} = (\boldsymbol{G}, \boldsymbol{E}, \boldsymbol{A})$ is used to represent the communication topology composed of n DC voltage droop control converter stations, and $\boldsymbol{G} = \{1, 2, \ldots, n\}$ is used to represent the node set of the communication network, $\boldsymbol{E} \in \boldsymbol{V} \times \boldsymbol{G}$ is the communication line between converter stations, and the neighbor converter station set of the GSVSCi converter station can be expressed as $\boldsymbol{N}_i = (j \in \boldsymbol{G} | (i, j) \in \boldsymbol{E})$, $\boldsymbol{A} = \{a_{ij}\} n \times n$ is the topology of communication network $\boldsymbol{G}$ between converter stations. If there is information transfer between two converter stations, then $a_{ij} \neq 0$, otherwise $a_{ij} = 0$.

2.2. AC side model of receiving converter station

The converter station at the receiving end of the VSC–MTDC system designed in this paper is connected with the strong AC power grid. The equivalent circuit of the grid side voltage source converter (GSVSC) is shown in Fig. 3. Among them, V_{cs} is the AC measured output voltage of the converter station and i_{dc} is the DC side output current.

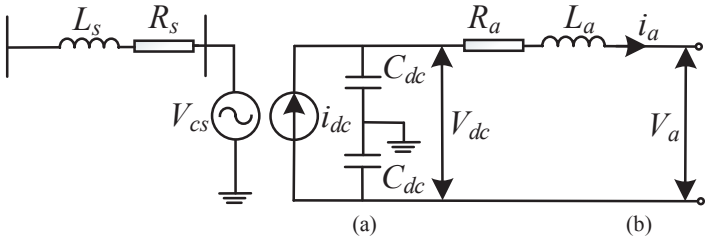

Fig. 3. GSVSC equivalent circuit: (a) AC side; (b) DC side

When the VSC–MTDC system is in a steady state, according to the analysis, the mathematical model of the GSVSCi converter station in the d–q synchronous rotating coordinate system can be obtained.

$$\begin{cases} L_{si} \dfrac{\mathrm{d}i_{sdi}}{\mathrm{d}t} = v_{sdi} - v_{di} - R_{si} i_{sdi} + w L_{si} i_{sqi} \\ L_{si} \dfrac{\mathrm{d}i_{sqi}}{\mathrm{d}t} = v_{sqi} - v_{qi} - R_{si} i_{sqi} + w L_{si} i_{sdi} \end{cases}. \tag{1}$$

By linearizing Eq. (1), the AC measurement model of the GSVSCi converter station can be obtained as:

$$\begin{cases} L_{si}\dfrac{\mathrm{d}\Delta i_{sdi}}{\mathrm{d}t} = -\Delta_{di} - R_{si}\Delta i_{sdi} + wL_{si}\Delta i_{sqi} \\ L_{si}\dfrac{\mathrm{d}\Delta i_{sqi}}{\mathrm{d}t} = -\Delta_{qi} - R_{si}\Delta i_{sqi} - wL_{si}\Delta i_{sdi} \end{cases}. \tag{2}$$

2.3. DC grid side model of receiving converter station

According to Fig. 3(b), the DC side of the GSVSC station is modeled, and the DC side equation is

$$\begin{cases} C_{\mathrm{dc}}\dfrac{\mathrm{d}V_{\mathrm{dc}}}{\mathrm{d}t} = \dfrac{P_{\mathrm{dc}}}{V_{\mathrm{dc}}} - i_a \\ L_a\dfrac{\mathrm{d}i_a}{\mathrm{d}t} = V_a - V_{\mathrm{dc}} - R_a i_a \end{cases}. \tag{3}$$

Formula (3) is expanded and linearized obtained.

$$\begin{cases} C_{\mathrm{dc}}\dfrac{\mathrm{d}V_{\mathrm{dc}}}{\mathrm{d}t} = \dfrac{1}{V_{\mathrm{dc},0}}\Delta P_{\mathrm{dc},0} - \dfrac{P_{\mathrm{dc},0}}{V_{\mathrm{dc},0}^2}\Delta V_{\mathrm{dc}} - \Delta i_a \\ L_a\dfrac{\mathrm{d}\Delta i_a}{\mathrm{d}t} = \Delta V_a - \Delta V_{\mathrm{dc}} - R_a\Delta i_a \end{cases}. \tag{4}$$

2.4. Modeling of converter station controller at receiving end

In the VSC–MTDC system designed in this paper, double closed-loop direct current control is adopted in the converter station control.

1) Inner loop controller model

The inner loop current controller adjusts the differential mode voltage of the upper and lower arms of the MMC, so that i_d can track the $i_{d\mathrm{ref}}$ output by the outer loop controller, and i_q can track the $i_{q\mathrm{ref}}$ output by the outer loop controller. At the same time, in the inner loop current controller, under the premise of considering the disturbance signals v_{sd} and v_{sq}, the feedforward decoupling strategy is used to decouple the d-axis and q-axis variables.

According to Fig. 4, it can be obtained.

$$\begin{cases} v_{di} = -\left(i_{d\mathrm{ref}i} - i_{sdi}\right)\left(k_{Ppi} + \dfrac{k_{Ipi}}{S}\right) \\ v_{qi} = -\left(i_{q\mathrm{ref}i} - i_{sqi}\right)\left(k_{Pqi} + \dfrac{k_{Iqi}}{S}\right) \end{cases}. \tag{5}$$

The state variables M_{di} and M_{qi} are introduced.

$$\begin{cases} M_{di} = \dfrac{k_{Ipi}}{S}\left(i_{d\mathrm{ref}i} - i_{sdi}\right) \\ M_{qi} = \dfrac{k_{Iqi}}{S}\left(i_{d\mathrm{ref}i} - i_{sqi}\right) \end{cases}. \tag{6}$$

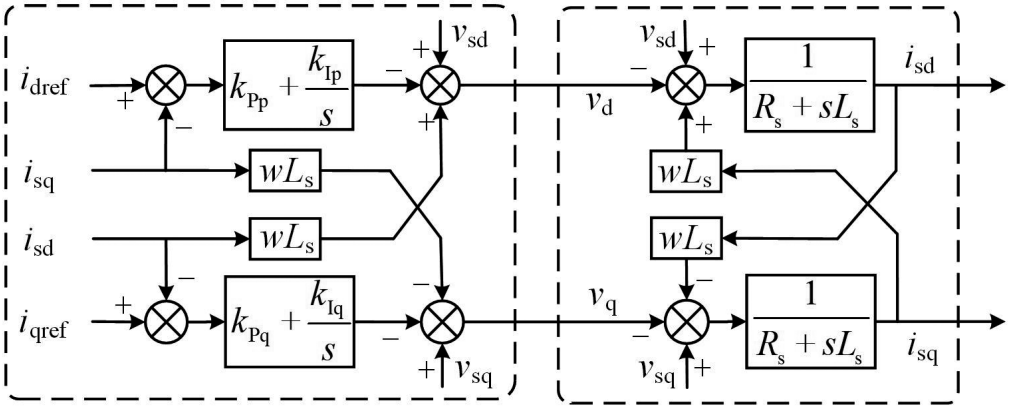

Fig. 4. Structure diagram of inner loop controller and mathematical model of VSC

Substituting Eq. (8) into Eq. (7), and linearizing the dynamic equation, we can get

$$\begin{cases} \dfrac{\mathrm{d}\Delta M_{di}}{\mathrm{d}t} = -k_{Ipi}\Delta i_{sdi} + k_{Ipi}\Delta i_{\mathrm{dref}i} \\ \dfrac{\mathrm{d}\Delta M_{qi}}{\mathrm{d}t} = -k_{Iqi}\Delta i_{sqi} + k_{Iqi}\Delta i_{\mathrm{qref}i} \\ \Delta v_{di} = -k_{Ppi}\Delta i_{sdi} - k_{Ppi}\Delta i_{\mathrm{dref}i} - \Delta M_{di} \\ \Delta v_{qi} = -k_{Pqi}\Delta i_{sqi} - k_{Pqi}\Delta i_{\mathrm{qref}i} - \Delta M_{qi} \end{cases} . \tag{7}$$

2) Outer loop controller model

The structure diagram of the outer loop controller is shown in Fig. 5. Among them, k_P and k_I are the proportional coefficient and integral constant of the PI controller, respectively.

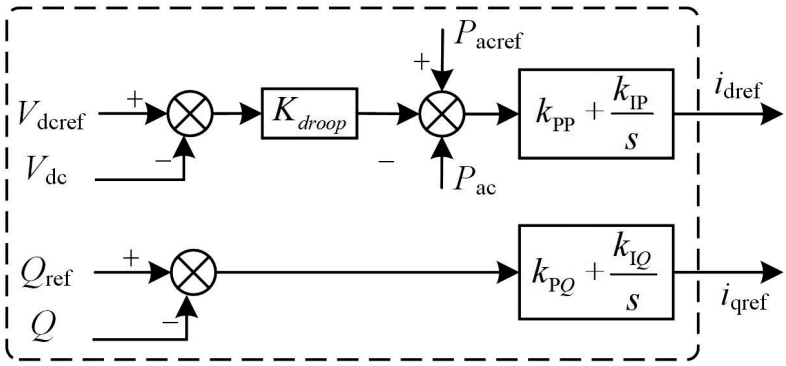

Fig. 5. Structure diagram of outer loop controller

According to the analysis shown in Fig. 5, the reference values $i_{d\mathrm{ref}i}$ and $i_{q\mathrm{ref}i}$ of the output active and reactive currents of the GSVSCi converter station can be obtained as:

$$\begin{cases} i_{d\mathrm{ref}i} = \left(P_{\mathrm{acref}i} - P_{\mathrm{ac}i} - K_{\mathrm{droop}i}V_{\mathrm{dc}i}\right)\left(k_{\mathrm{PP}i} + \dfrac{k_{IPi}}{S}\right) \\ i_{q\mathrm{ref}i} = \left(Q_i - Q_{\mathrm{ref}i}\right)\left(k_{PQi} + \dfrac{k_{IQi}}{S}\right) \end{cases}. \tag{8}$$

The state variables M_{Pi} and M_{Qi} are introduced as:

$$\begin{cases} M_{Pi} = \dfrac{k_{IPi}}{S}\left(P_{\mathrm{acref}i} - P_{\mathrm{ac}i} - K_{\mathrm{droop}i}V_{\mathrm{dc}i}\right) \\ M_{Qi} = \dfrac{k_{IQi}}{S}\left(-Q_i - Q_{\mathrm{ref}i}\right) \end{cases}, \tag{9}$$

and let

$$\begin{cases} P_{\mathrm{ac}i} = v_{si}i_{sdi} \\ Q_i = v_{si}i_{sqi} \end{cases}. \tag{10}$$

Substituting Formula (11) and Formula (12) into Formula (10), and linearizing the dynamic equation, we can get

$$\begin{cases} \dfrac{\mathrm{d}\Delta M_{Pi}}{\mathrm{d}t} = -k_{IPi}v_{si}\Delta i_{sdi} - k_{IPi}K_{\mathrm{droop}i,0}\Delta V_{\mathrm{dc}i} - k_{IPi}V_{\mathrm{dc}i,0}\Delta K_{\mathrm{droop}i} \\ \dfrac{\mathrm{d}\Delta M_{Qi}}{\mathrm{d}t} = -k_{PQi}v_{si,0}\Delta i_{sqi} \\ \Delta i_{d\mathrm{ref}i} = -k_{\mathrm{PP}i}v_{si}\Delta i_{sdi} - k_{\mathrm{PP}i}K_{\mathrm{droop}i,0}V_{\mathrm{dc}i} - k_{\mathrm{PP}i}V_{\mathrm{dc}i}\Delta K_{\mathrm{droop}i} + \Delta M_{Pi} \\ \Delta i_{q\mathrm{ref}i} = -k_{PQi}V_{si,0}\Delta i_{sqi} + \Delta M_{Qi} \end{cases}. \tag{11}$$

2.5. VSC–MTDC subsystem model

According to Eqs. (2), (4), (7) and (11), the linear state space model of the receiving end for the GSVSCi converter station can be obtained as:

$$\frac{\mathrm{d}\Delta \boldsymbol{x}_{gsi}}{\mathrm{d}t} = \boldsymbol{A}_{gsi}\Delta \boldsymbol{x}_{gsi} + \boldsymbol{B}_{gsi}\Delta \boldsymbol{u}, \tag{12}$$

where: the state variable is $\Delta \boldsymbol{x}_{gsi} = [\Delta V_{\mathrm{dc}i}, \Delta i_{sdi}, \Delta i_{sdi}, \Delta M_{di}, \Delta M_{qi}, \Delta M_{Pi}, \Delta M_{Qi}]$; the input variable is $\Delta \boldsymbol{u}_{gsi} = \Delta K_{\mathrm{droop}i}$.

In the distributed collaborative optimization control strategy proposed in this paper, in order to better verify the absorption effect of the system on renewable energy with randomness and fluctuation, the sending end converter station adopts constant active power control mode and constant AC voltage control mode, the sending end converter station controller adopts double closed-loop direct current control, and the double closed-loop control block diagram of the sending end converter station is shown in Fig. 6.

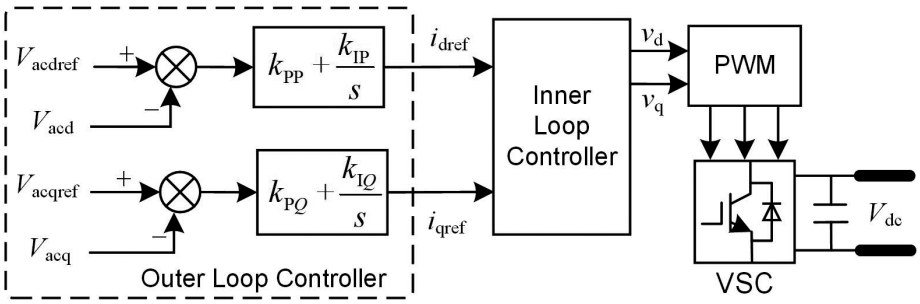

Fig. 6. Double closed loop control block diagram of sending end converter station

Considering that the system mainly realizes the optimal control of DC grid voltage through the cooperative control of the receiving converter station, the modeling of the sending converter station controller is not included in the system modeling in the process of establishing the distributed system model. At the same time, the main converter station is controlled by the DC voltage margin controller, and the dynamic characteristics of the controller have little influence on the distributed model controller, so its dynamic characteristics are not included in the system modeling. Finally, the linear state space model for the droop control converter station subsystem is established as follows:

$$\begin{cases} \dfrac{\mathrm{d}\Delta \boldsymbol{x}_i}{\mathrm{d}t} = \boldsymbol{A}_i \Delta \boldsymbol{x}_i + \boldsymbol{B}_i \Delta \boldsymbol{u}_i + \boldsymbol{E}_i \Delta \boldsymbol{d}_i + \sum\limits_{j=1, j\neq i} \left(\boldsymbol{A}_{ij} \Delta \boldsymbol{x}_j + \boldsymbol{B}_{ij} \Delta \boldsymbol{u}_j \right) \\ \Delta \boldsymbol{y}_i = \boldsymbol{C}_i \Delta \boldsymbol{x}_i \end{cases}, \tag{13}$$

where: $\Delta \boldsymbol{x}_i$, $\Delta \boldsymbol{u}_i$, $\Delta \boldsymbol{d}_i$ and $\Delta \boldsymbol{y}_i$ represent the state variable, control input, disturbance variable and output variable of the GSVSCi subsystem area of the converter station, respectively. $\boldsymbol{A}_i$, $\boldsymbol{B}_i$, $\boldsymbol{E}_i$, and $\boldsymbol{C}_i$ are the state matrix, control matrix, disturbance matrix and observation matrix of the GSVSCi converter station, respectively. $\boldsymbol{A}_{ij}$ and $\boldsymbol{B}_{ij}$ are the coupling matrices between the GSVSCi converter station and the GSVSCj converter station. $\Delta \boldsymbol{x}_i = [\Delta V_{\mathrm{dc}i}, \Delta i_{sdi}, \Delta i_{sdi}, \Delta M_{di}, \Delta M_{qi}, \Delta M_{Pi}, \Delta M_{Qi}, \Delta V_{gs\mathrm{dc}i}]$, $\Delta \boldsymbol{u}_i = \Delta K_{\mathrm{droop}i}$, $\Delta \boldsymbol{d}_i = \Delta V_{gs\mathrm{dc}}$.

According to Eq. (15), the discrete linear state space model of the converter station subsystem I with end suspension control is

$$\begin{cases} \dfrac{\mathrm{d}\Delta \boldsymbol{x}_i(k+1)}{\mathrm{d}t} = \boldsymbol{A}_{di} \Delta \boldsymbol{x}_i(k) + \boldsymbol{B}_{di} \Delta \boldsymbol{u}_i(k) + \boldsymbol{E}_{di} \Delta \boldsymbol{d}_i(k) \\ \qquad\qquad + \sum\limits_{j=1, j\neq i} \left(\boldsymbol{A}\, \boldsymbol{d}_{ij} \Delta \boldsymbol{x}_j(k) + \boldsymbol{B}_{dij} \Delta \boldsymbol{u}_j(k) \right) \\ \Delta \boldsymbol{y}_i(k) = \boldsymbol{C}_{di} \Delta \boldsymbol{x}_i(k) \end{cases}, \tag{14}$$

where: $\boldsymbol{A}_{di}$, $\boldsymbol{B}_{di}$, $\boldsymbol{E}_d$, $\boldsymbol{C}_{di}$, $\boldsymbol{A}_{dij}$ and $\boldsymbol{B}_{dij}$ are the corresponding matrices of $\boldsymbol{A}_i$, $\boldsymbol{B}_i$, $\boldsymbol{E}_i$, $\boldsymbol{C}_i$, $\boldsymbol{A}_{ij}$ and $\boldsymbol{B}_{ij}$ after discretization, respectively.

3. Design of distributed model predictive controller

3.1. Distributed prediction model and control objective

The prediction model of the subsystem i for the receiving end droop control converter station is expressed as:

$$\begin{cases} \dfrac{\mathrm{d}\Delta \boldsymbol{x}_i(k+h+1\,|k)}{\mathrm{d}t} = \boldsymbol{A}^h \boldsymbol{L}_i \Delta \boldsymbol{x}_i(k) + \boldsymbol{A}^h \boldsymbol{L}_i' \Delta \boldsymbol{x}_i(k) + \sum_{s=1}^{h} \boldsymbol{A}^{s-1} \boldsymbol{B}_{di} \Delta \boldsymbol{u}_i(k+h|k) \\ \qquad\qquad \boldsymbol{E}_{di} \Delta \boldsymbol{d}_i(k) + \sum_{j=1, j\neq i}^{n} \sum_{s=1}^{h} \boldsymbol{A}^{s-1} \boldsymbol{B}_{dj} \Delta \boldsymbol{u}_i(k+n|k-1) \\ \Delta \boldsymbol{y}_i(k+h+1||k) = \boldsymbol{C}_{di} \Delta \boldsymbol{x}_i\,(k+h+1|k) \end{cases}, \tag{15}$$

where: $\boldsymbol{L}_i = [0_{ni\times a}\ I_{ni}\ 0_{ni\times b}]$, I_{ni} is the n_i-order unit matrix; $\boldsymbol{L}_I' = \text{diagonal}([\boldsymbol{I}_a\ 0_{ni}\ \boldsymbol{I}_b])$, $\boldsymbol{I}_a$ and $\boldsymbol{I}_b$ are the a-order and b-order unit matrices, respectively; $\boldsymbol{B}_i = [\boldsymbol{B}^{T\,1i}\ \boldsymbol{B}^{T\,2i} \ldots \boldsymbol{B}^{T\,ni}]^T$.

The optimized performance indicators of the subsystem i for the droop control converter station is as follows:

$$\min J_i(k) = \sum_{h=1}^{P} \left\| V_i\left(k+h|k - \hat{V}(k+h|k)\right)\right\|_{\boldsymbol{Q}_i}^2 + \sum_{h=1}^{C} \|\Delta u_i(k+h-1|k)\|_{\boldsymbol{R}_i}^2\,, \tag{16}$$

where: P is the prediction time domain, C is the control time domain, $\boldsymbol{Q}_i$ and $\boldsymbol{R}_i$ are positive definite weighting matrices, and $V(k+h|k)$ is the set value of DC voltage.

$$\begin{cases} V_{i\,\min}(k+h|k) \le V_{i\,\max}(k+h|k) \\ \Delta u_{i\,\min}(k+h|k) \le \Delta u_i(k+h-1|k) \le \Delta u_{i\,\max}(k+h|k) \end{cases}. \tag{17}$$

Equation (19) ensures that the DC side voltage of the converter station and the change value of the droop coefficient of the converter station do not exceed the set value.

3.2. DMPC problem solving based on ADMM algorithm

In the process of the Di-MPC rolling optimization solution in this paper, the alternating direction method of multipliers (ADMM) is used to solve the distributed optimization problem and improve the efficiency of the solution.

1) QP form of DMPC problem

The problem of the Di-MPC optimization problem of the receiving end droop control converter station can be transformed into a QP problem. In each sampling, the online local. The objective function $J_i(k)$ is decomposed into two sub-problems, $F(x)$ and $G(z)$, and the distributed controller solves the QP optimization problem at the sampling time k as follows:

$$\min J_i(k) = F(x) + G(z) = \frac{1}{2}\boldsymbol{X}^T \boldsymbol{H}\, \boldsymbol{X} + \boldsymbol{Q}^T \boldsymbol{X}, \tag{18}$$

where: $F(x)$ and $G(z)$ are the convex functions, $\boldsymbol{H}$ and $\boldsymbol{Q}$ are the objective function coefficient matrices, respectively.

2) QP problem solving based on ADMM algorithm

The optimization problem is transformed into the ADMM standard form as follows:

$$\begin{cases} \min & F(x)+G(z) \\ \text{s.t} & \boldsymbol{A}_i x+\boldsymbol{B}_i z=C \end{cases}, \tag{19}$$

where: $x \in R^n$ is the original variable, and $z \in R^m$ is the auxiliary variable. $\boldsymbol{A}_i$, $\boldsymbol{B}_i$ and $\boldsymbol{C}$ are the coupling coefficient matrices, $\boldsymbol{A}_i \in R^{p\times n}$, $\boldsymbol{B}_i \in R^{p\times m}$, $\boldsymbol{C} \in R^p$.

The augmented Lagrangian function is constructed as follows:

$$L_\rho(x,z,u)=F(x)+G(z)+u^T\ (\boldsymbol{A}_i x+\boldsymbol{B}_i z-C)+\frac{\rho}{2}\left\|\boldsymbol{A}_i x+\boldsymbol{B}_i z-C\right\|, \tag{20}$$

where $\rho>0$ is the penalty coefficient, u is the Lagrange multiplier.

On this basis, the alternating direction method of multipliers is used to iteratively solve the optimal control problem.

3.3. Distributed model predictive controller

In the process of predictive control, Di-MPC mainly includes predictive model, rolling optimization and feedback correction [20]. The distributed model predictive controller of the droop control converter station designed in this paper is shown in Fig. 7. Where: K'_{droop} is the corrected value of the droop coefficient.

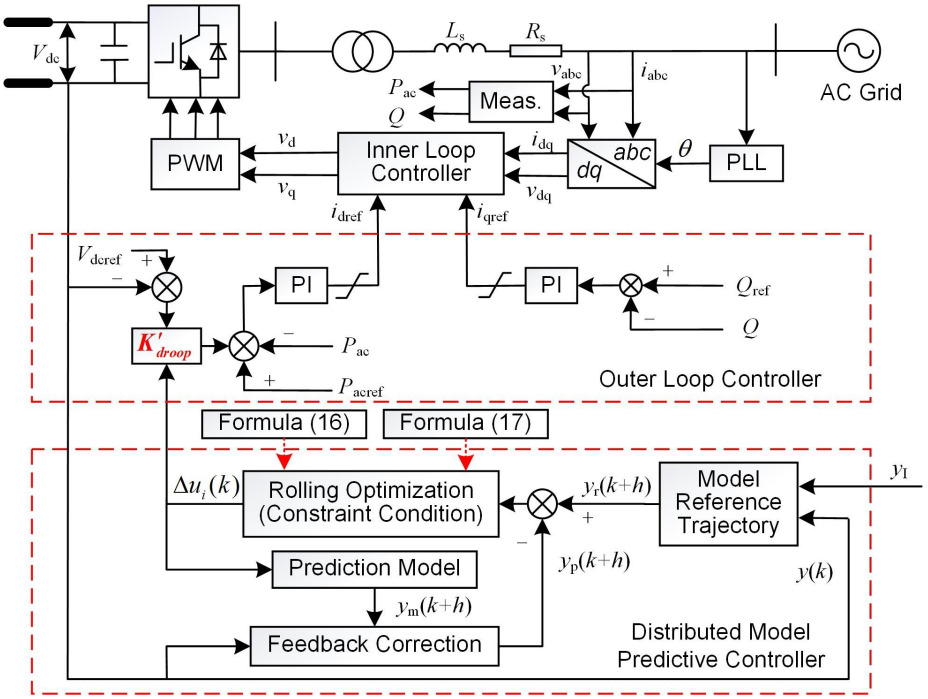

Fig. 7. Distributed model predictive controller for droop control converter station

4. Distributed cooperative optimization of DC voltage control strategy

The VSC–MTDC system with renewable energy access can be divided into two types according to the different systems connected to the AC side of each converter station. The converter station with new energy access on the AC side is called the sending end converter station; The converter station connected with the strong AC system is called the receiving converter station. The workflow of the system control strategy is shown in Fig. 8. The sending end converter station includes the WF-VSC connected with a wind farm and the PV-VSC connected with a photovoltaic power station, which adopts constant active power control mode for control, and tracks the instantaneous maximum output active power according to MPPT to maximize the utilization of renewable energy such as wind power and photovoltaic [20]. The converter station at the receiving-end is connected with the strong AC system, which mainly balances the DC power fluctuation caused by the randomness and fluctuation of wind power and solar energy, and stabilizes the DC voltage of the system. In the setting process of the receiving converter station, the converter station with the largest capacity is selected as the main GSVSC station, and the voltage margin controller is used for control. The GSVSCi droop control converter station ($I = 1, \ldots, n$) is used as the auxiliary converter station, and the converter station adopts the Di-MPC method based on cooperative control.

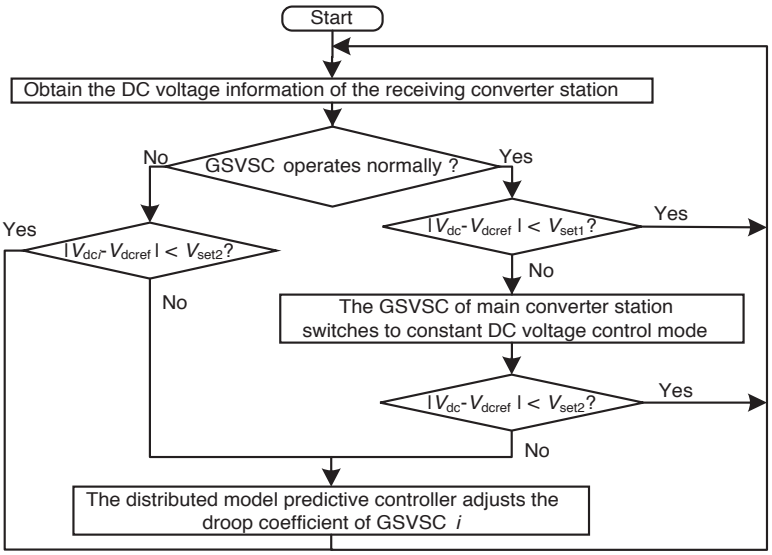

Fig. 8. Workflow chart of control strategy

When the GSVSC works normally: the WF-VSC and PV-VSC at the sending end of the system have relatively small fluctuations in the injected power, and when the DC voltage deviation of the GSVSC at the receiving end of the main converter station $|V_{dc} - V_{dc\,ref}|$ is less than the preset value V_{set1}, the GSVSCi droop control converter station assumes the DC voltage control task, the GSVSC works in constant power control mode. When the GSVSC DC voltage deviation $|V_{dc} - V_{dc\,ref}|$ is less than the preset value V_{set2} and greater than V_{set1}, the main GSVSC station

switches to the constant DC voltage control mode and assumes the DC voltage control task. When the DC voltage deviation of GSVSC DC voltage $|V_{\mathrm{dc}} - V_{\mathrm{dc\,ref}}|$ is greater than the preset value V_{set2}, the GSVSCi droop control converter station adopts a cooperative Di-MPC method to control GSVSCi, and the distributed model predictive controller is exchanged. The droop coefficient of the converter station is adjusted to maintain the system's DC voltage within the allowable working range, and the main GSVSC station still undertakes the task of DC voltage control.

When the GSVSC is out of operation: the GSVSCi droop control converter station jointly undertakes the system DC voltage control. The input power of the converter station at the receiving end of the system fluctuates, resulting in a change in the DC voltage of the converter station at the receiving end. When the DC voltage deviation $|V_{\mathrm{dc}i} - V_{\mathrm{dc\,ref}}|$ is less than the preset value V_{set2}, the droop coefficient of the droop control converter station does not change, and the DC voltage remains within the allowable operating range at this time. When the DC voltage deviation of the receiving end converter station $|V_{\mathrm{dc}i} - V_{\mathrm{dc\,ref}}|$ is greater than the preset value V_{set2}, the system adopts a collaborative Di-MPC method based on the cooperative type to perform collaborative control on the receiving end droop control converter station.

5. Simulation analysis

5.1. Simulation description

The six-terminal flexible HVDC system is shown in Fig. 9. The system includes six converter stations. Among them, the WF-VSC and PV-VSC stations are used as the sending end and connected to wind farms and photovoltaic power stations respectively; the GSVSC1, GSVSC2, GSVSC3 and GSVSC stations are used as the receiving end converter stations. Additionally, they are connected to the strong AC power grid. According to regulations, in order to ensure the safe and stable operation of the VSC–MTDC system, the fluctuation range of the DC grid voltage

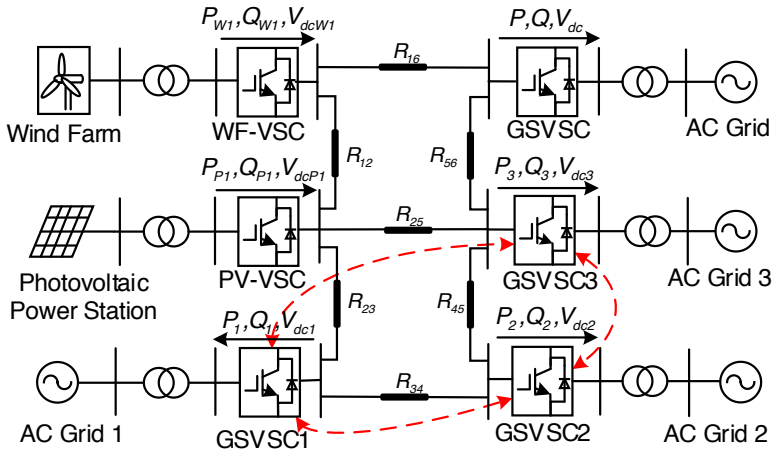

Fig. 9. Six terminal flexible DC transmission system

should be ±0.05 pu. The system simulation parameters are shown in Table 1. For convenience, the simulation results of this paper have standardized the DC voltage and active power values.

Table 1. System simulation parameters

Parameter name	Symbol	Value	Unit
Rated DC voltage	$V_{\mathrm{dc\,ref}}$	400	kV
Reference of DC voltage	V_{ref}	400	kV
Reference value of active power	P_{ref}	500	MW
DC side capacitance	C_{dc}	800	μF
AC side equivalent resistance	R_s	0.025	Ω
AC side equivalent reactance	L_s	73	mH
DC side bridge arm resistance	R_a	2	Ω
DC side bridge arm reactance	L_a	60	mH
Rated active capacity	WF-VSC	2	pu
Rated active capacity	PV-VSC	2	pu
Rated active capacity	GSVSC1	0.6	pu
Rated active capacity	GSVSC2	0.8	pu
Rated active capacity	GSVSC3	1.2	pu
Rated active capacity	GSVSC	1.4	pu
Preset value of DC voltage deviation	V_{set1}	0.01	pu
Preset value of DC voltage deviation	V_{set2}	0.03	pu

5.2. The system operates normally

Example 1: The remaining margin of the main GSVSC station can bear the unbalanced power.

In the initial state. The power injected into the DC grid from wind farms and photovoltaic power plants is 1.0 pu and 0.8 pu, respectively. At 4.5 s, the power injected by the WF-VSC into the DC grid will increase from 1.0 pu to 1.1 pu. At 6.5 s, the power injected by the WF-VSC into the DC grid will increase from 1.1 pu to 1.5 pu. The simulation curve of the converter station when the input power fluctuates is shown in Figs. 10(a) and 10(b).

According to the simulation results, in the proposed control strategy, when the output fluctuation of wind farms and photovoltaic power stations is small, the droop control converter station undertakes unbalanced power distribution and stabilizes the DC voltage of the system. When the DC side voltage deviation of the GSVSC in the main converter station is greater than 0.01 pu, its working mode will be switched to constant DC voltage control to undertake system DC voltage control. Although there is a small deviation in DC voltage, it can effectively avoid the DC voltage stability problem caused by droop coefficient adjustment.

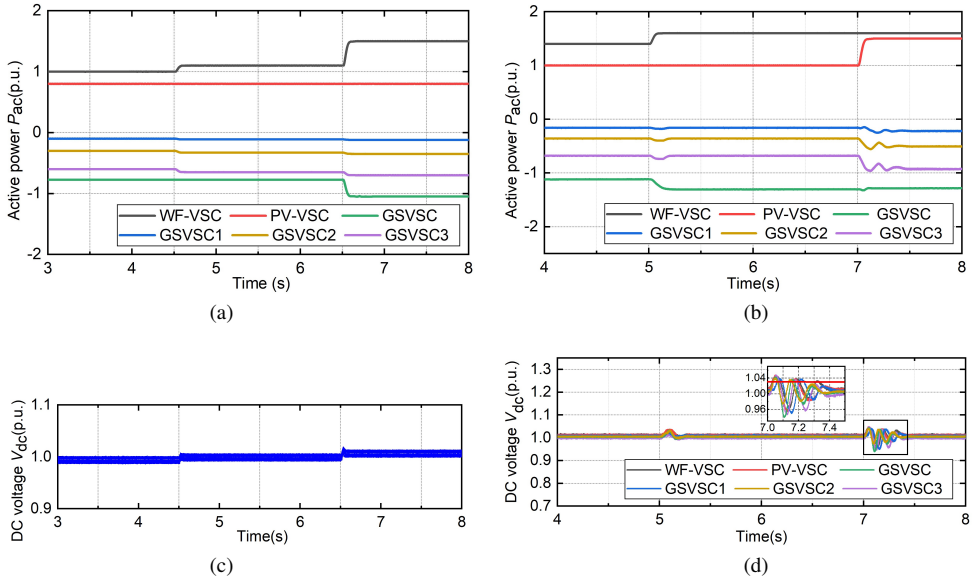

Fig. 10. Simulation curve of VSC with input power fluctuation simulation curve of VSC: (a) active power curve of VSC; (b) DC voltage curve of VSC; (c) active power curve of VSC; (d) DC voltage curve of VSC

Example 2: The remaining margin of the main GSVSC station is not enough to bear the unbalanced power.

In the initial state, the MTDC system operates stably. At 5.0 s, the power injected by WF-VSC into the DC grid will increase from 1.4 pu to 1.8 pu. At 7.0 s, the PV-VSC will inject DC power the grid power is increased from 1.0 pu to 1.4 pu. The simulation curve of the converter station of the VSC–MTDC system is shown in Figs. 10(c) and 10(d).

The simulation results show that when the residual margin of GSVSC in the main converter station can bear the unbalanced power, the DC voltage of the system remains stable. When the residual margin of the GSVSC in the main converter station is insufficient, the unbalanced power of the system is jointly borne by GSVSC1, GSVSC2 and GSVSC3 converter stations. The droop control converter station adjusts the droop coefficient to reduce the DC grid voltage deviation of the converter station.

The next part mainly focuses on the analysis of the constant droop coefficient control and the variable droop coefficient control, and the control performance under the active power fluctuation working conditions at the sending end. Among them, the variable droop coefficient adjusts the droop coefficient of the receiving end droop control converter station through two different control methods: centralized model predictive control (CMPC) and Di-MPC.

In the initial state, the VSC–MTDC system operates stably, taking the input active power fluctuation of Example 2 as a reference. At 7 s, when the operating state and power fluctuation value are the same as in Example 2, three different control methods, namely, the fixed droop coefficient, CMPC and Di-MPC are used to control the system. The comparison chart of DC voltage simulation curves of the VSC with different control strategies is shown in Fig. 11.

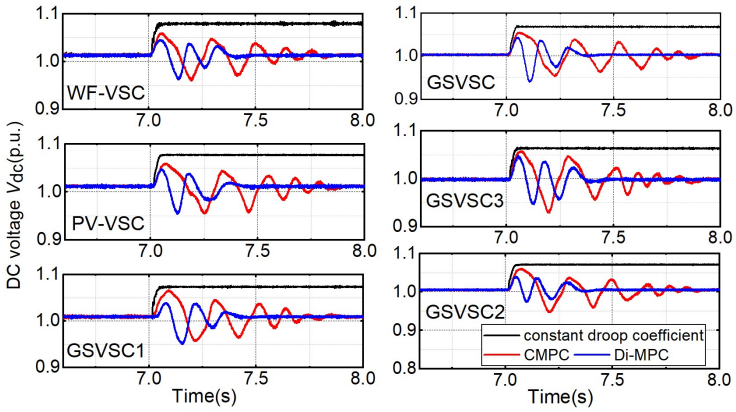

Fig. 11. Comparison of DC voltage simulation curves of VSC with different control strategies

From the analysis of the comparison chart of the DC voltage simulation curve of each converter station, it can be seen that for the fixed droop coefficient control method, when the input power of the sending end increases too much, the DC voltage rises sharply and exceeds the set value, resulting in a large DC voltage deviation. Both CMPC and Di-MPC can adjust the droop coefficient of the droop control converter station to restore the DC grid voltage to the steady-state value before power fluctuation and reduce the DC voltage deviation. Compared with the CMPC, the Di-MPC has a faster DC voltage response speed, smaller fluctuation value, shorter recovery time and better dynamic performance. When the system adopts different control strategies, the control effect data comparison is shown in Table 2.

Table 2. Comparison of control effect data of different control strategies

Control strategy	**Time of adjustment t (s)**	**DC voltage deviation of main converter station value (pu)**
Constant droop coefficient	0.045	0.078
CMPC	0.85	0.013
Di-MPC	0.44	0.014

5.3. System fault condition

Example 1: The GSVSC1 converter station exits operation.

In the initial state, the VSC–MTDC system operates stably. At 5 s, the GSVSC1 receiving-end converter station fails, and the converter station transmits 0 to the AC grid. At 6 s, the GSVSC1 receiving-end converter station returns to normal. The power delivered by the converter station to the AC grid is restored to a input power value of 0.2 pu before the failure. The simulation curve of the converter station of the VSC–MTDC system is shown in Figs. 12(a) and 12(b).

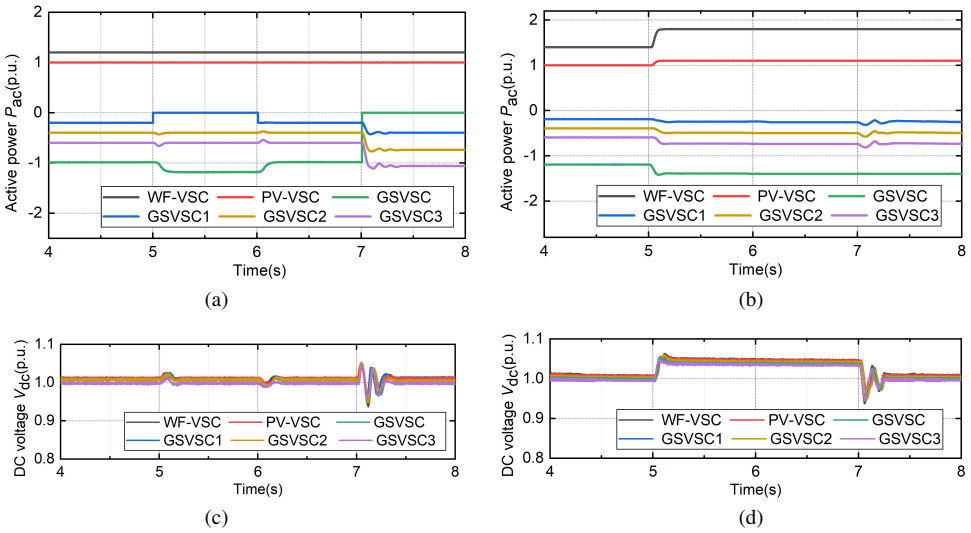

Fig. 12. Simulation curve of VSC under system fault condition: (a) active power curve of VSC under out of operation condition; (b) DC voltage curve of VSC under out of operation condition; (c) active power curve under system communication fault condition; (d) DC voltage curve under system communication fault condition

In the proposed control strategy, the main GSVSC station uses a voltage margin controller for control. When the system power fluctuation value does not exceed the main converter station's own capacity, the unbalanced power caused by the shutdown and access of the GSVSC1 converter station is all borne by the main converter station, and the system DC voltage remains stable.

Example 2: The main converter station exits operation.

At 7 s, the main converter station itself fails, and it no longer delivers power to the AC grid. The simulation curve of the VSC–MTDC system is shown in Figs. 12(c) and 12(d).

According to the analysis of the simulation results, the unbalanced power caused by the shutdown of the GSVSC of the main converter station will be borne by the droop control converter station. When the DC voltage deviation exceeds the set value, the receiving droop control converter station adjusts the droop coefficient of the converter station through distributed model predictive control to restore the DC grid voltage to the expected value.

Example 3: System communication failure.

In the initial state, the system operates stably, and the injected DC power of the wind farm and photovoltaic power station is 1.4 pu and 1.0 pu, respectively. At 5 s, the system has communication failure. At this time, the injection power of the WF-VSC to the DC power grid increases from 1.4 pu to 1.8 pu, and the injection power of the PV-VSC to the DC power grid increases from 1.0 pu to 1.1 pu. At 5 s, the system communication returns to normal. The simulation curve of the converter station of the VSC–MTDC system is shown in Figs. 12(c) and 12(d).

According to the analysis of the simulation results, under the condition of communication failure, the system can still maintain stable operation within a certain power fluctuation range, but

the deviation between DC grid voltage and reference values is large. After the system communication is restored, the sag coefficient of the converter station will be adjusted to improve the DC voltage control accuracy of the system.

6. Conclusion

Aiming at the problems of power system's DC grid voltage control deviation and instability caused by large-scale renewable energy access to the VSC–MTDC, this paper combines the advantages of DC voltage margin control and DC voltage droop control, and proposes a distribution based on a sparse communication network that cooperatively optimizes the DC voltage control strategy. The proposed control strategy effectively reduces the number of droop coefficient adjustments, avoids the instability of DC voltage control caused by frequent droop coefficient adjustments, and reduces the DC grid voltage control deviation. The simulation results show that:

1. When the DC voltage deviation does not exceed the preset value, the unbalanced power generated by the fluctuation of the renewable energy output in the system will be borne by the main converter station, effectively avoiding the DC grid voltage caused by the frequent adjustment of the droop coefficient. Fluctuations ensure the stability of the system's DC voltage control.
2. When the DC voltage deviation exceeds the preset value, the receiving end droop control converter station adjusts the droop coefficient of the droop control converter station through a cooperative Di-MPC method to quickly restore the DC voltage to the desired DC voltage value, so that the system DC voltage control has better dynamics and accuracy.
3. For the receiving converter station of the VSC–MTDC system, including the main converter station and droop control converter station, as well as any receiving converter station out of operation and system communication failure, the proposed control strategy can still maintain the stable operation of the system.

Acknowledgements

This work was supported in part by the Key Research and Development Project of Gansu Province under Grant 18YF1GA056, and in part by the Tianyou innovation team of Lanzhou Jiaotong University under Grant TY202009.

References

[1] Xu D., Liu Y., Wu J., *Review on Control Strategies of Multi-Terminal Direct Current Transmission System*, Transactions of China Electrotechnical Society, vol. 30, no. 17, pp. 1–12 (2015), DOI: 10.1109/TSTE.2015.2497340.

[2] Su M.H., Li Y.K., Dong H.Y., Liu K.Q., Zou W.W., *Subsynchronous oscillation and its mitigation of VSC–MTDC with doubly-fed induction generator-based wind farm integration*, Archives of Electrical Engineering, vol. 70, no. 1, pp. 53–72 (2021), DOI: 10.24425/aee.2021.136052.

[3] Liu T.Q., Tao Y., Li B.H., *Critical Problems of Wind Farm Integration via MMC-MTDC System*, Power System Technology, 2017, vol. 41, no. 10, pp. 1–9 (2017).

[4] Li C.S., Li Y.K., Guo J., He P., *Research on emergency DC power support coordinated control for hybrid multi-infeed HVDC system*, Archives of Electrical Engineering, vol. 69, no. 1, pp. 5–21 (2020), DOI: 10.24425/aee.2020.131755.

[5] Wang L., Wu X.L., Hou J.X., Wang T.Z., *Control of photovoltaic power integration based on multi-terminal VSC HVDC system*, Power System Protection and Control, vol. 47, no. 4, pp. 65–72 (2019).

[6] Suo Z.W., Li G.Y., Chi Y.G., Wang W.S., *Multi-port DC Substation for Offshore Wind Farm Is Master-slave Control*, Automation of Electric Power Systems, vol. 39, no. 11, pp. 16–23 (2015).

[7] Nakajima T., Irokawa S.A., *control system for HVDC transmission by voltage sourced converters*, 1999 IEEE Power Engineering Society Summer Meeting, Conference Proceedings, pp. 1113–1119 (1999).

[8] Wang Z., He J.H., Yin X., Fang Z., *Distributed Control of VSC–MTDC Systems Considering Tradeoff Between Voltage Regulation and Power Sharing*, IEEE Transactions on Power Systems. vol. 35, no. 3, pp. 1812–1821 (2020), DOI: 10.1109/TPWRS.2019.2953044.

[9] Eduardo P.A., Agusti E.A., Sajjad F. *et al*., *DC voltage droop control design for multi-terminal HVDC systems considering AC and DC grid dynamics*, 2016 IEEE Power and Energy Society General Meeting2 (2016), DOI: 10.1109/PESGM.2016.7741218.

[10] Xiao L., Xu Z., An T., Bian Z.P., *Improved Analytical Model for the Study of Steady State Performance of Droop-Controlled VSC–MTDC Systems*, IEEE Transactions on Power Systems, vol. 32, no. 3, pp. 2083–2093 (2017), DOI: 10.1109/TPWRS.2016.2601104.

[11] Wang K., Liu J.T., Li Y.P., Zeng D., *An adaptive power control strategy based droop feedback for VSC-HVDC Review on Control Strategies of Multi-Terminal Direct Current Transmission System*, Power System Protection and Control, vol. 42, no. 9, pp. 48–53 (2014).

[12] Wang Y.Z., Wen W.J., Wang C.S. *et al*., *Adaptive Voltage Droop Method of Multiterminal VSC-HVDC Systems for DC Voltage Deviation and Power Sharing*, IEEE Transactions on Power Delivery, 2019, vol. 34, no. 1, pp. 169–176 (2019), DOI: 10.1109/TPWRD.2018.2844330.

[13] Chen P., Li M.H., Yan B., Hao J.F., Zhang Q., Zhao Q., *Flexible Droop Control Strategy for VSC–MTDC Systems*, Power System Technology, vol. 40, no. 11, pp. 3433–3440 (2016).

[14] Wu J.L., Liu X.H., Wang X.W., Yao W.Z., *Research of DC Voltage Hybrid Control Strategy for VSC–MTDC System*, Power System Technology, vol. 39, no. 6, pp. 1593–1599 (2015).

[15] Wang Z.D., Li K.J. *et al*., *A Coordination Control Strategy of Voltage-Source-Converter-Based MTDC for Offshore Wind Farms*, IEEE Transactions on Industry Applications, 2015, vol. 51, no. 4, pp. 2743–2752 (2015), DOI: 10.1109/TIA.2015.2407325.

[16] Yan M., Cai H., Xie Z.J., Zhang Z.R., Xu Z., *Distributed DC voltage control strategy for VSC–MTDC systems*, Electric Power Automation Equipment, vol. 40, no. 3, pp. 134–140 (2020), DOI: 10.16081/j.epae.202002011.

[17] Sun G.Q., Zheng Y.P., Wei Z.N., Zang H.X., Lin Z.J., Yuan Y., *Model predictive control strategy for MMC-MTDC with offshore wind farms considering droop control characteristic*, Renewable Energy Resources, vol. 35, no. 3, pp. 419–426 (2017).

[18] Li G.Y., Du Z.C., Shen C. *et al*., *Coordinated Design of Droop Control in MTDC Grid Based on Model Predictive Control*, IEEE Transactions on Power Systems, 2018, vol. 33, no. 3, pp. 2816–2828 (2018), DOI: 10.1109/TPWRS.2017.2764112.

[19] Eriksson R., *A New Control Structure for Multiterminal DC Grids to Damp Interarea Oscillations*, IEEE Transactions on Power Delivery, 2016, vol. 31, no. 3, pp. 990–998 (2016), DOI: 10.1109/TPWRD.2014.2364738.

[20] Le J., Liao X.B., Zhang Y.T., Chang J.X., Lu J., *Review and Prospect on Distributed Model Predictive Control Method for Power System*, Automation of Electric Power Systems, 2020, vol. 44, no. 23, pp. 179–191 (2020).

[21] Zhang Q.Z., Wang B., Li Y., Liu C., *Research on fault crossing coordination control of a wind farm via a flexible direct current transmission system*, Transactions of China Electrotechnical Society, 2020, vol. 48, no. 10, pp. 131–138 (2020).